

# $\pi^0 \rightarrow e^+e^-e^+e^-$ Analysis Summary

P. Toale

November 6, 2007

This document summarizes the current state of the  $\pi^0 \rightarrow 4e$  analysis. My thesis will serve as the long writeup <sup>1</sup>. There are three measurements to report on. First, an improved branching ratio measurement, making use of higher statistics and including first order radiative corrections. Then there is a three dimensional fit to the differential decay spectrum from which we extract both the DIP form factor parameter and the parity.

The same signal data are used for both measurements. The branching ratio measurement also relies on a normalization mode. The signal mode is  $K_L \rightarrow \pi_{\gamma\gamma}^0 \pi_{\gamma\gamma}^0 \pi_{4e}^0$ , which I refer to as DD. The normalization mode is  $K_L \rightarrow \pi_{\gamma\gamma}^0 \pi_{ee\gamma}^0 \pi_{ee\gamma}^0$ , referred to as 2D. The two modes have identical final states consisting of four electrons and four photons.

## 1 Summary of Changes

There have been several modifications to numbers and results presented in my thesis that I summarize here. There have been two important improvements made to systematic errors, one in the branching ratio result and one in the parity measurement. The chamber resolution systematic has been re-evaluated with V600 MC with improved statistics, and has changed from 0.84 % to 0.11 %. The error on the  $\eta$  parameter due to the resolution of the angle  $\phi$  was previously 0.084 and is now 0.030.

In addition, there were several mistakes discovered in my thesis. First, the double ratio for the Win97 dataset was miscalculated as 0.2263; it should be 0.2269. This changes the combined ratio from 0.2244 to 0.2245. Second the systematic associated with MC statistics should have been 0.25 % instead

---

<sup>1</sup><http://kpsa.fnal.gov:8080/public/ktev-theses.html#pat>

Table 1: Selection cuts.

Variable	Accepted Range
Minimum Cluster Energy	$> 2 \text{ GeV}$
Total CsI Energy	$40 - 210 \text{ GeV}$
Minimum Cluster Separation	$> 5 \text{ cm}$
Minimum Track Momentum	$> 2 \text{ GeV}/c$
$E/p$	$0.93 - 1.07$
$\chi^2_{\text{vertex}}$	$< 40$
$\chi^2_{\text{magnet}}$	$< 100$
$z$ -Vertex Position	$94 - 157 \text{ m}$
Total Invariant Mass	$480 - 515 \text{ MeV}/c^2$
$P_T^2$	$< 800 \text{ MeV}^2/c^2$
Pairing $\chi^2$	$< 12$
Minimum Track Separation	$> 2 \text{ mm}$

of the stated 0.26 %. Lastly, the weighted average of the  $\kappa$  parameter was quoted as  $-0.008$  when it should have been  $-0.011$ .

The limits on the mixing angle  $\zeta$  have changed in two ways. The decreased uncertainty on  $\eta$  decreases the limit allowing for CPT violation from  $11.3^\circ$  to  $5.7^\circ$ , while the increased significance of  $\kappa$  increases the limit assuming CPT violation from  $1.7^\circ$  to  $1.9^\circ$ .

## 2 Data Processing

The data used for both measurements were collected by the 2eNclus trigger, selected in the 4track channel of the crunch, and further filtered to have 8 total clusters, 4 associated with tracks and 4 not associated with tracks. Additional cuts were made to define the final event sample. These include fiducial cuts, kinematic cuts, and background cuts. Table 1 lists the cuts.

Events are classified as signal or normalization mode based on the follow-

Table 2: Acceptances.

Mode	Win97	Sum97	99
$\epsilon_{DD}^{DD}$	$1.957(9) \cdot 10^{-3}$	$1.935(11) \cdot 10^{-3}$	$3.211(9) \cdot 10^{-3}$
$\epsilon_{DD}^{2D}$	$2.59(11) \cdot 10^{-5}$	$2.78(13) \cdot 10^{-5}$	$5.13(12) \cdot 10^{-5}$
$\epsilon_{2D}^{DD}$	$1.90(16) \cdot 10^{-6}$	$2.13(21) \cdot 10^{-6}$	$3.25(14) \cdot 10^{-6}$
$\epsilon_{2D}^{2D}$	$2.131(5) \cdot 10^{-3}$	$2.124(7) \cdot 10^{-3}$	$3.266(4) \cdot 10^{-3}$
$\epsilon_{1D}^{DD}$	$0.89(19) \cdot 10^{-8}$	$1.23(28) \cdot 10^{-8}$	$1.73(16) \cdot 10^{-8}$
$\epsilon_{1D}^{2D}$	$3.64(39) \cdot 10^{-8}$	$6.41(64) \cdot 10^{-8}$	$8.38(36) \cdot 10^{-8}$

ing  $\chi^2$  quantities,

$$\chi_{DD}^2 = \frac{(M_{4e} - M_{\pi^0})^2}{\sigma_{4e}^2} + \frac{(M_{\gamma\gamma 1} - M_{\pi^0})^2}{\sigma_{\gamma\gamma}^2} + \frac{(M_{\gamma\gamma 2} - M_{\pi^0})^2}{\sigma_{\gamma\gamma}^2}, \quad (1a)$$

$$\chi_{2D}^2 = \frac{(M_{ee\gamma 1} - M_{\pi^0})^2}{\sigma_{ee\gamma}^2} + \frac{(M_{ee\gamma 2} - M_{\pi^0})^2}{\sigma_{ee\gamma}^2} + \frac{(M_{\gamma\gamma} - M_{\pi^0})^2}{\sigma_{\gamma\gamma}^2}. \quad (1b)$$

The smaller of the two is defined as the pairing  $\chi^2$  and classifies the event. The measured resolutions on the masses are:  $\sigma_{\gamma\gamma} = 1.6$  MeV,  $\sigma_{ee\gamma} = 1.7$  MeV, and  $\sigma_{4e} = 2.1$  MeV.

The acceptance after all cuts is a product of the efficiencies at trigger (6–8%), crunch (25–37%), filter (26–28%), and analysis cuts (43–50%). The final acceptance for both signal and normalization mode events from three sources is listed in Table 2, where  $\epsilon_y^x$  is the acceptance of source  $y$  reconstructed as mode  $x$ . The sources are signal MC, normalization MC, and single-Dalitz background MC (1D). These sources include the two major backgrounds: cross-over events (signal reconstructed as normalization and vice-versa) and conversion events. The signal mode acceptance is defined as the number of reconstructed events divided by the number of events generated with  $x_{4e} = M_{4e}^2/M_{\pi^0}^2 > 0.9$ .

Table 3 lists the number of candidate events in each mode along with the ratio of signal mode to normalization mode ( $r$ ). The statistical error on the ratio in the combined dataset is 0.63%.

Table 3: Final event sample and ratio  $r = N_{DD}/N_{2D}$ .

	Win97		Sum97		99		Total	
	2D	DD	2D	DD	2D	DD	2D	DD
Events	26011	5429	19879	4152	95361	20930	141251	30511
$r$	0.2087(31)		0.2089(36)		0.2195(17)		0.2160(14)	

Table 4: The double ratio  $R$  in each dataset with statistical errors. The three run periods produce consistent results with a  $\chi^2$  of 2.2 for 2 degrees of freedom.

Dataset	$R$
Win97	$0.2269 \pm 0.0034$
Sum97	$0.2289 \pm 0.0039$
99	$0.2230 \pm 0.0017$
Combined	$0.2245 \pm 0.0014$

### 3 Branching Ratio

The branching ratio is derived from the observed ratio of DD to 2D events. This is directly related to the branching ratio  $\Gamma(\pi^0 \rightarrow 4e)/\Gamma^2(\pi^0 \rightarrow ee\gamma)$ ,

$$R = r \frac{\epsilon_{2D}^{2D}}{\epsilon_{DD}^{DD}} = \frac{\Gamma(\pi^0 \rightarrow 4e)\Gamma(\pi^0 \rightarrow \gamma\gamma)}{\Gamma^2(\pi^0 \rightarrow ee\gamma)},$$

where  $r = N_{DD}/N_{2D}$ .

This formula can be modified to explicitly account for any residual background,

$$R = \frac{(r\epsilon_{2D}^{2D} - \epsilon_{2D}^{DD}) + \frac{1}{\rho}(r\epsilon_{1D}^{2D} - \epsilon_{1D}^{DD})}{\epsilon_{DD}^{DD} - r\epsilon_{DD}^{2D}},$$

where  $\rho = \Gamma_{ee\gamma}/\Gamma_{\gamma\gamma} = 0.01213$  is the PDG value of the single Dalitz branching ratio. Table 4 summarizes the calculated value of the double ratio  $R$ . The errors are a combination of the statistical error on the data and the statistical errors on the MC acceptances. The weighted average is  $R = 0.2245 \pm 0.0014$ .

With the value of  $R$  now calculated, we can extract the expected level of background contamination in the final event sample. Table 5 lists the number of candidate events in each mode, the amount of background estimated from

Table 5: Estimate of residual background and final event sample.

	Win97		Sum97		99		Total	
	2D	DD	2D	DD	2D	DD	2D	DD
Total	26011	5429	19879	4152	95361	20930	141251	30511
XO	71	23	59	20	332	94	462	137
1C	36	9	49	9	201	41	286	59
Signal	25904	5397	19771	4123	94828	20795	140503	30315

Table 6: Summary of Systematic Uncertainties. Statistical error is 0.62 %.

Source	Error (%)
MC Stats	0.25
Cut Var	0.21
Material	0.15
Backgrounds	0.15
DC Res	0.11
$\delta_{\text{rad}}$	0.04
DC Ineff	0.04
CsI Res	0.02
$\mathcal{M}(\alpha, \zeta, \delta)$	0.01
Total Uncertainty	0.41

Monte Carlo, and the number of background subtracted events. After all cuts there remains a small level ( $\sim 0.6\%$ ) of background contamination.

### 3.1 Systematic Studies

Since the signal and normalization modes have the same final state, it is expected that most systematic errors will cancel in the ratio. The sources of error that have been studied are listed in Table 6. Two of the values have changed since my thesis. First the MC statistical error should have been 0.25 % instead of 0.26 %. More importantly, the chamber resolution error has been re-evaluated, changing from 0.84 % to 0.11 %. The combined systematic error is 0.41% and the total uncertainty is 0.74%. For comparison, the total error quoted in my thesis was 1.11 %.

### 3.1.1 Cut Variation

Each cut was varied independently over a reasonable range around the nominal value. Excesses of more than one uncorrelated statistical error were added in quadrature. The error in the Win97 period was mainly due to  $E/p$ , while in the Sum97 run period it was the minimum cluster separation. All excesses were small for the 99 dataset. The combined error was 0.21%.

### 3.1.2 Detector Material

Previous E799 measurements of the amount of material in the detector concluded that the composition of helium bag 1A was known to 5%. The ratio of acceptances was measured over the full range from all air to all helium and was seen to change by 3%. A systematic error of 5% of this variation, or 0.15%, was assigned.

### 3.1.3 Background Estimate

The background acceptances are small ( $10^{-5}$  for XO and  $10^{-8}$  for 1C). In order to limit the systematic error due to residual background, their acceptances were allowed to vary individually by a factor of 2. The variation that resulted in the largest change in the double ratio changed it by 0.15%.

### 3.1.4 Chamber Resolution

The original chamber resolution study used independent MC datasets with hits smeared such that the central part of the SOD distributions were wider or narrower by 10%. The ratio of acceptance was seen to change by 0.84% over this range.

New MC was generated with the smearing of hits turned off. During reconstruction, the hits were smeared by various amounts from 0 to  $\sim 300 \mu\text{m}$ , and the ratio of acceptances was calculated. Figure 1 shows the dependence of the acceptance ratio on the level of hit smearing for the three run periods. The linear fits imply an error on the ratio of 1.14% of the uncertainty on the intrinsic hit resolution.

The plan is to study how the width of the  $E/p$  distribution of high- $p$  tracks changes as the smearing changes in order to limit the uncertainty in the resolution. For now, I will just claim the uncertainty is 10% and quote a systematic error on the double ratio of 0.11%. This results in a total error

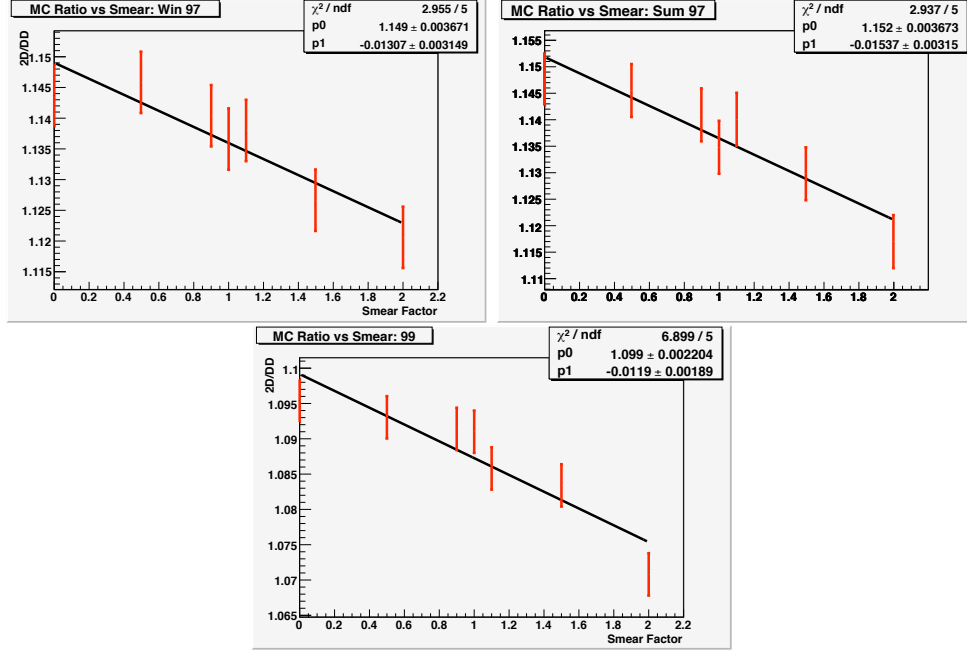


Figure 1: Acceptance ratio as a function of smear factor, from no smearing to twice nominal smearing.

on the branching ratio of 0.74%. If the chamber resolution error doubles to 0.22%, the total error increases to only 0.75%.

### 3.1.5 Radiative Corrections

The simulation includes first order radiative corrections for both the signal and normalization modes. The error in neglecting higher order radiative effects was estimated by taking the square of the difference between tree-level and 1st order, resulting in an error of 0.04%.

### 3.1.6 Chamber Inefficiencies

The inefficiency of a plain-pair is measured in the data and stored in a DCMAP for use in the simulation. Chamber illuminations were used to limit the uncertainty in the scale factor applied to the map to less than 20%. Monte Carlo data was then reweighed with scale factors of 20% larger and

smaller than the nominal value. The ratio of acceptances changed by 0.04% over this range.

### 3.1.7 Calorimeter Energy Resolution

The uncertainty in the energy resolution of the calorimeter was estimated by looking at the run-to-run variation in the width of the  $E/p$  distribution. This width was seen to vary by 1%. The cluster energy of MC events was smeared such that the  $E/p$  distribution was 1% wider than nominal. The ratio of acceptances changed by 0.02%.

### 3.1.8 Matrix Element

The signal mode acceptance depends on the assumed form of the  $\pi^0\gamma^*\gamma^*$  coupling. The acceptance was calculated over a range of coupling parameters (set by the measured uncertainty) and was found to vary by no more than 0.01%.

## 3.2 Results

The branching ratio that we will quote is,

$$\frac{\Gamma(\pi^0 \rightarrow 4e, x_{4e} > 0.9)}{\Gamma^2(\pi^0 \rightarrow ee\gamma)} = 0.2272 \pm 0.0014 \text{ (stat)} \pm 0.0009 \text{ (syst)}.$$

The Monte Carlo predicts that the branching ratio for  $x_{4e} > 0.9$  is 94.202 % of the total  $\Gamma(\pi^0 \rightarrow 4e) + \Gamma(\pi^0 \rightarrow 4e\gamma)$  branching ratio. Extrapolating to all values of  $x_{4e}$  I find,

$$\frac{\Gamma(\pi^0 \rightarrow 4e(\gamma))}{\Gamma^2(\pi^0 \rightarrow ee\gamma)} = 0.2412 \pm 0.0018.$$

To compare to the previous results, one can fold in the single-Dalitz branching ratio but must pay the price of its uncertainty,

$$\Gamma(\pi^0 \rightarrow 4e, x_{4e} > 0.9) = (3.26 \pm 0.18) \times 10^{-5}.$$

## 4 Parity and Form Factor Fit

A three dimensional fit was preformed on the signal data sample to extract the DIP form factor parameter and to limit the size of a scalar coupling in the matrix element. The coupling at the  $\pi^0\gamma^*\gamma^*$  vertex is given by,

$$C_{\mu\nu\rho\sigma} \propto f(x_1, x_2; \alpha) [\cos \zeta \epsilon_{\mu\nu\rho\sigma} + e^{i\delta} \sin \zeta (g_{\mu\rho}g_{\nu\sigma} - g_{\mu\sigma}g_{\nu\rho})],$$

where the first term in square brackets is the standard pseudoscalar coupling and the second term is a scalar coupling. The admixture is described by a mixing angle  $\zeta$  and phase difference  $\delta$ . The form factor parametrization used is the DIP model with an added constraint,  $\beta = -(1 + 2\alpha)$ ,

$$f_{DIP}(x_1, x_2; \alpha) = \frac{1 - \mu(1 + \alpha)(x_1 + x_2)}{(1 - \mu x_1)(1 - \mu x_2)},$$

where  $\mu = M_{\pi^0}^2/M_\rho^2 \approx 0.032$  and  $x_{1,2} = q_{1,2}^2/M_{\pi^0}^2$  is the moment transfer of the virtual photon. For small  $x$ , there is a relationship between the traditional  $\pi^0$  slope parameter and the DIP parameter,  $a = -\mu\alpha$ .

A more suitable form of the coupling is obtained through the following change of variables,

$$\begin{aligned}\kappa &= \tan \zeta \cos \delta, \\ \eta &= \tan \zeta \sin \delta.\end{aligned}$$

With this transformation, the coupling is,

$$C_{\mu\nu\rho\sigma} \propto \frac{f(x_1, x_2; \alpha)}{\sqrt{1 + \kappa^2 + \eta^2}} [\epsilon_{\mu\nu\rho\sigma} + (\kappa + i\eta) (g_{\mu\rho}g_{\nu\sigma} - g_{\mu\sigma}g_{\nu\rho})].$$

The tree-level matrix element is symmetric in  $\eta$ , so only the region  $\eta \geq 0$  will be explored.

### 4.1 Likelihood Function

The function that will be minimized is,

$$L(\vec{\mu}) = - \sum_i^{N_{data}} \ln f(\vec{x}_i; \vec{\mu}),$$

where  $\vec{x}$  is the set of five phase space variables,  $\vec{\mu}$  is the set of fit parameters, and where the sum runs over reconstructed events. The function  $f$  is just the normalized differential partial width,  $f \propto d\Gamma(\vec{x}, \vec{\mu})/d\vec{x}$ . The normalization is the observed partial width at a given value of  $\vec{\mu}$ , which can be calculated from MC. The reconstructed sample consists of both  $\pi^0 \rightarrow 4e$  events and  $\pi^0 \rightarrow 4e\gamma$  events.

$$\Gamma_{obs}(\vec{\mu}) = \frac{1}{N_{gen}^{4e}} \sum_i^{N_{mc}^{4e}} \frac{d\Gamma_{4e}(\vec{x}_i; \vec{\mu})}{d\vec{x}_i} + \frac{1}{N_{gen}^{4e\gamma}} \sum_i^{N_{mc}^{4e\gamma}} \frac{d\Gamma_{4e\gamma}(\vec{y}_i; \vec{\mu})}{d\vec{y}_i},$$

where the sums run over reconstructed MC events of each type.

It is convenient to factor the differential partial width into an amplitude, which depends on  $\vec{\mu}$ , and a phase space term, independent of  $\vec{\mu}$ . The normalization can then be computed by calculating the amplitude at each value of  $\vec{\mu}$  and reweighting,

$$\Gamma_{obs}(\vec{\mu}) = \frac{1}{N_{gen}^{4e}} \sum_i^{N_{mc}^{4e}} \frac{A_{4e}(\vec{x}_i; \vec{\mu})}{A_{4e}(\vec{x}_i; \vec{\mu}_{gen})} W(\vec{x}_i, \vec{\mu}_{gen}) + \frac{1}{N_{gen}^{4e\gamma}} \sum_i^{N_{mc}^{4e\gamma}} \frac{A_{4e\gamma}(\vec{y}_i; \vec{\mu})}{A_{4e\gamma}(\vec{y}_i; \vec{\mu}_{gen})} W(\vec{y}_i, \vec{\mu}_{gen}),$$

where  $W$  is the contribution of the event to the differential partial width evaluated at  $\vec{\mu}_{gen}$ .

In the numerator of  $f$ , the phase space term can be ignored since it simply adds a constant to  $L$ . The amplitude which is used is the  $\pi^0 \rightarrow 4e$  amplitude, but with a large photon energy cutoff. The cutoff is chosen to correspond to  $x_{4e} = 0.9$  which is  $E_\gamma^* = 6.8$  MeV. So the final form of the likelihood function is,

$$L(\vec{\mu}) = - \sum_i^{N_{data}} \ln \frac{A_{4e}^{E_{cut}}(\vec{x}_i; \vec{\mu})}{\Gamma_{obs}(\vec{\mu})},$$

## 4.2 MC Studies

Large samples of MC events with known  $\vec{\mu}$  were used to test the fit and study the properties of the likelihood function near the minimum. The fit successfully extracted the input values of two of the parameters,  $\alpha$  and  $\kappa$ , with distributions consistent with the curvature of the likelihood. The third parameter,  $\eta$ , was found to suffer a systematic bias which can be attributed to the finite resolution on the angle  $\phi$  between the Dalitz pairs.

The differential partial width with respect to  $\phi$  is,

$$\frac{d\Gamma}{d\phi} \sim 1 - A \cos 2\phi + B \sin 2\phi,$$

where  $A$  and  $B$  can be written as,

$$\begin{aligned} A &\sim -0.2 \cos 2\zeta, \\ B &\sim +0.2 \sin 2\zeta \cos \delta. \end{aligned}$$

On the  $\eta$ -axis, near the origin, these become,

$$\begin{aligned} A &\sim -0.2(1 - 2\eta^2), \\ B &\sim 0. \end{aligned}$$

Therefore, a non-zero  $\eta$  along with  $\kappa = 0$  will induce a standard  $\cos 2\phi$  oscillation, but with a reduced amplitude. The finite resolution on  $\phi$  manifests itself in exactly the same way. So the fit compensates for the smeared amplitude by increasing  $\eta$ . This is corrected for by mapping out the functional relationship between  $\eta_{input}$  and  $\eta_{extracted}$  in MC and applying it to the extracted value in data.

The other important quantity characterized by the MC is the distribution of the values of the likelihood function at the minimum, normalized by the number of events used in the fit. This distribution can be used as a goodness-of-fit characterization.

### 4.3 Fit Values

The signal data set was fit and the minimum of the likelihood function was seen to agree well with the MC distribution, indicating that the function is in fact a good description of the data. The extracted values are shown in Table 7.

### 4.4 Systematic Errors

The same set of systematics described above were also studied for the likelihood fit analysis. Additionally, there is an error associated with the MC normalization calculation as well as with the resolution bias on  $\eta$ . Table 8 lists the systematic uncertainties on the three fit parameters. Below I detail the significant systematic uncertainties.

Table 7: Raw fit results with statistical errors.

Dataset	$\alpha$	$\kappa$	$\eta$
Win97	$-0.2 \pm 2.3$	$-0.020 \pm 0.020$	$0.113 \pm 0.073$
Sum97	$-1.8 \pm 2.6$	$-0.034 \pm 0.024$	$0.151 \pm 0.063$
99	$+2.3 \pm 1.2$	$-0.003 \pm 0.011$	$0.135 \pm 0.031$
Combined	$+1.3 \pm 1.0$	$-0.011 \pm 0.009$	$0.135 \pm 0.026$

Table 8: List of significant systematic uncertainties on the fit parameters.

Source	$\alpha$	$\kappa$	$\eta$
Norm	0.31	0.005	0.006
$\phi$ Bias			0.030
Cuts	0.87	0.010	0.006
Total	0.93	0.011	0.031

#### 4.4.1 Normalization

In order to estimate the error in the normalization calculation, the MC dataset was split into 5 parts and each was used to calculate a new normalization. The fit was then done with the 5 independent normalizations. The error associated with the normalization calculation was taken as the largest single deviation out of the 5 subsets, divided by  $\sqrt{5}$ . This resulted in an error on  $\alpha$ ,  $\kappa$ , and  $\eta$  of, 0.31, 0.0048, and 0.0060, respectively.

#### 4.4.2 Resolution Bias

The correction for the resolution bias on  $\eta$  was mapped out using MC. For the measured value of  $\eta$  given above the size of the correction is 0.084. Allowing for a 10% uncertainty in the parametrization of the correction, the correction itself has an error of 0.030.

#### 4.4.3 Cut Variation

The cut variation study was done in exactly the same way as for the branching ratio measurement. The errors on  $\alpha$ ,  $\kappa$ , and  $\eta$  were 0.874, 0.0103, and 0.0057, respectively.

Table 9: Fit results with combined errors. The corrected value of  $\eta$  is shown.

Parameter	Value
$\alpha$	$1.3 \pm 1.4$
$\kappa$	$-0.011 \pm 0.014$
$\eta$	$0.05 \pm 0.03$

## 4.5 Results

The final values, with  $\eta$  corrected, and showing total uncertainties, are listed in Table 9. Since  $\eta$  is constrained to be positive, a limit is derived using the prescription of Feldman and Cousins,

$$\eta \leq 0.10 \quad \text{at 90 \% CL.}$$

With  $\eta$  consistent with zero, the phase  $\delta$  is unconstrained. I will calculate two limits on the mixing angle, one allowing for CPT violation and one assuming CPT is conserved. For the first, I take  $\eta$  at its upper limit, along with the measured value of  $\kappa$ , and find,

$$\zeta \leq 5.7^\circ \quad \text{allowing CPT violation.}$$

For the second limit, I fix  $\eta$  to be zero and calculate the 90 % CL limit on  $|\kappa|$ ,

$$|\kappa| \leq 0.034 \quad \text{at 90 \% CL.}$$

I then find,

$$\zeta \leq 1.9^\circ \quad \text{requiring CPT conservation.}$$